Maas, H. J.; Naber, A.; Fuchs, H.; Fischer, U. C.; Weeber, J. C.; Dereux, A.
Imaging of photonic nanopatterns by scanning near-field optical microscopy, *Journal of the Optical Society of America B-Optical Physics*, 2002; 19 (6):1295-1300.

http://hdl.handle.net/2440/37491

Imaging of photonic nanopatterns by scanning near-field optical microscopy

H. J. Maas, A. Naber, H. Fuchs, and U. C. Fischer

Physikalisches Institut, Westfälische Wilhelms-Universität, Münster, Germany

J. C. Weeber and A. Dereux

Laboratoire de Physique, Optique Submicronique, Université de Bourgogne, Dijon, France

We define photonic nanopatterns of a sample as images recorded by scanning near-field optical microscopy with a locally excited electric dipole as a probe. This photonic nanopattern can be calculated by use of the Green's dyadic technique. Here, we show that scanning near-field optical microscopy images of well-defined gold triangles taken with the tetrahedral tip as a probe show a close similarity to the photonic nanopattern of this nanostructure with an electric dipole at a distance of 15 nm to the sample and tilted 45° with respect to the scanning plane. © 2002 Optical Society of America

OCIS codes: 180.5810, 240.4350, 110.2990, 100.6640.

1. INTRODUCTION

The characterization of surfaces at a nanometric scale has recently attracted much attention in the context of imaging the local distribution of optical properties such as the photoluminescence or the dielectric properties beyond the diffraction limit of light microscopy by scanning near-field optical microscopy[1–5] (SNOM). Apart from imaging the local distribution of the complex dielectric constant, the imaging of a surface is relevant to obtain insight into the behavior of electromagnetic fields at the nanometer scale,[6] e.g., in the case of photonic band structures.[7–9] It was observed previously that the pattern displayed in SNOM images depends strongly on the polarization of the light emitted from the SNOM probe.[5,10–12] Here we define a photonic nanopattern of a sample as a nanoscopically resolved SNOM image of this sample recorded with a locally excited dipole as a probe. This photonic nanopattern can be calculated by use of the Green's dyadic technique. SNOM on the basis of the tetrahedral tip (T-tip) proved to be a useful method to obtain microscopic information of optical properties of a surface at a resolution in the 10-nm range.[13–15] Here, we demonstrate how this technique can be used for imaging the characteristic photonic nanopattern of a well-defined structure with an electric dipole tilted 45° with respect to the scanning plane at a resolution scale of <50 nm. In previous experiments the dipolar nature of dye molecules was used to map the near-field distribution of SNOM fiber tips.[16,17] In this study, we show that applying this dipolar character to the tip itself allows us to model the complex optical contrast of SNOM images taken with a T-tip over extended objects.

2. EXPERIMENTAL BACKGROUND

To prepare a T-tip, a glass fragment must be first broken out of a cover slip. A corner of this fragment is the tip of a tetrahedron, which forms the transparent body of the T-tip. The tip is coated with gold by a two-state evaporation process. One of the three edges (K1) of the tetrahedron is coated with a layer of gold thinner than the rest of the tip.[13,14] Local light emission from the T-tip is thought to be generated by optical excitation of surface plasmons along the special edge K1.[18] The excitation of a local surface plasmon of a gold particle at the tip acts finally as a nanoscopic light source for SNOM. With the T-tip, a resolution capability of <50 nm was first demonstrated in a purely optical mode (inverse photon scanning tunneling microscope).[13] Subsequently, in a configuration with scanning tunneling microscopy distance control, optical image details smaller than 10 nm became observable.[14,15,19] However, in the scanning tunneling microscopy mode, only conductive samples can be investigated. To overcome this restriction, a dynamic scanning force microscopy (SFM) feedback based on a piezoelectric quartz tuning fork as a force sensor[20–22] has recently been implemented[23,24] and is used here for the first time for SNOM with the T-tip.

Figure 1 shows the setup. The T-tip has to be fixed on one prong of the tuning fork, as can be seen in Fig. 1(a). A tiny prism has to be attached to the rear of the glass fragment for shining light into the body of the tip along the axis *A*. For this purpose, the tuning fork and the T-tip must be tilted 45° with respect to the surface. Figure 1(b) shows the optical set up. The light of a laser diode *LD* (λ = 635 nm) is focused into the T-tip. A polarizer *P* guarantees a linear polarization direction, which is in the plane of incidence as is defined by the axis *A* and the edge K1 of the T-tip. The light transmitted through the sample *S* into the far-field is collected by an objective *O* of 0.55 numerical aperture.

For the investigation of photonic nanopatterns a latex-bead projection sample of gold is particularly suitable.[25–27] The samples are prepared by use of a
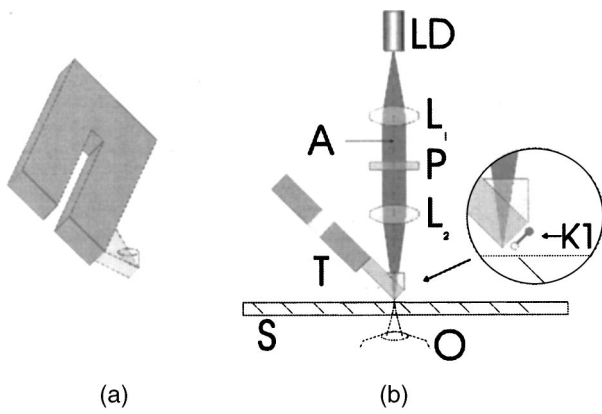
(a)   (b)

Fig. 1.   Schematic of the experimental setup.

nearly complete close-packed monolayer of uniform latex beads of a diameter of 220 nm as a mask for evaporation of a 15–20-nm-thick film of gold onto mica. Gold triangles arranged in hexagonal symmetry are formed in this way. The gold structure is covered with a spin-coated film of polycarbonate (PC) and a glass cover slip. After removal of the mica the characteristic gold structure embedded into PC is exposed. The periodicity of the hexagonally arranged triangles (220 nm) is below half the wavelength of the light used (635 nm), whereas the triangles with a size of ~50 nm are larger than the resolution limit of the T-tip. To suppress topographic artifacts[28] as far as possible, the projection sample is embedded in the surface of a thin transparent film of polycarbonate (PC).

3. RESULTS AND DISCUSSION

Figure 2 shows simultaneously taken SFM and SNOM images of a projection pattern.[29] In the SFM image [Fig. 2(a)], the typical structure of hexagonally arranged triangles appears as slight depressions of a depth of ~1 nm. The SNOM image [Fig. 2(b)] also shows a hexagonal formation, but the shape of individual spots deviates significantly from that of the triangular gold patches. The triangle in the upper marked area is associated with a bright spot in the center and a dark spot at the apex of the pattern. The oppositely oriented triangle in the lower marked area has a totally different appearance with a less-pronounced contrast. The contrast alternates with the two opposite orientations of the triangles. Thus the orientation of the T-tip with respect to the triangles seems to play an important role for the resulting contrast. Other features in the SFM image of Fig. 2(a) are ringlike depressions and a circular hole in the polymer film. These depressions are replicas of accidental residues of the latex mask occurring in the fabrication process of the sample.[27] As these topographic features do not appear in the SNOM image [Fig. 2(b)], the conclusion can be drawn that the optical signal is not significantly influenced by a topographical artifact.

Another example, which was obtained on a different sample, is shown in Fig. 3. In the SFM image [Fig. 3(a)] the gold triangles appear as slight protrusions. The two marked areas show two triangles with the same mutual orientation. The corresponding areas in the SNOM im-

age [Fig. 3(b)] exhibit the same optical contrast. Both patterns show the same change of bright and dark spots obviously deviating from the local distribution of gold. The triangles have a different orientation with respect to the probing tip compared with the one of Fig. 2. The axis connecting the two triangles is rotated by 15° to the horizontal direction in contrast to the situation in Fig. 2, where the axis is rotated by roughly 90°. As a result of this different orientation, the triangles appear with a different contrast.

Previous observations gave us a first clue to an understanding of the puzzling contrast. The emission from the T-tip is at its maximum, when the beam irradiating the tip is polarized in the plane of incidence as defined by the incoming beam and the special edge K1 [see Fig. 4(a)]. Therefore the polarization of the incident beam is always chosen to be in this plane of incidence (coinciding with the paper plane); otherwise, the optical contrast decreases and can even completely vanish for a perpendicular polarization.[15] Thus the special edge shapes the excitation of the tip. We previously made an attempt to interpret SNOM images by assuming that the near-field emission from the T-tip can be considered as a dipole emission and that the SNOM contrast is caused by an interference of the emission of the dipole with its mirror image in the sample.[14] Similar considerations lead us now to the assumption that the emission from the T-tip may be represented by a radiating dipole oriented parallel to the special edge of the T-tip and thus tilted by 45° with respect to the surface [see Fig. 4(a)]. The effect of such a dipole on

(a)   (b)
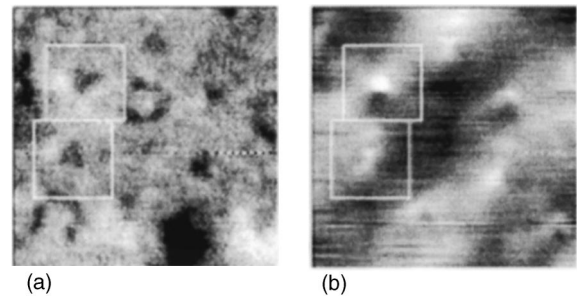
Fig. 2.   15-nm-thick gold projection sample embedded in polycarbonate: scan size is 400 nm × 400 nm.   (a) SFM image; the gray scale corresponds to 6 nm.   (b) SNOM image; the maximum contrast in this image is 0.3%.

(a)   (b)
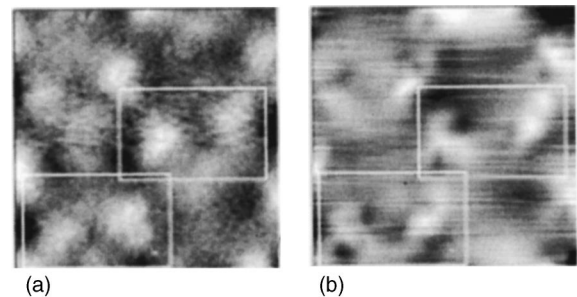
Fig. 3.   Image of a sample with a gold structure of 20 nm thickness showing the effect of a different orientation of the triangles with respect to the probing tip: (a) SFM image; scan size 480 nm × 480 nm; the gray scale corresponds to a height of 4.3 nm.   (b) Simultaneously recorded SNOM image; the image contrast is 1%.
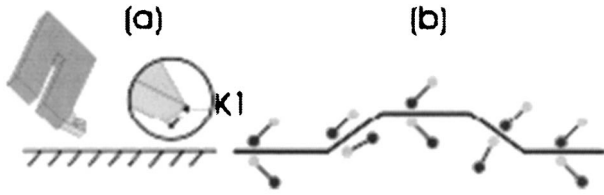
Fig. 4. (a) Scheme of the T-tip attached to a quartz tuning fork. The special edge K1 is tilted 45° to the sample surface. (b) The tilted dipole model: the dipole induces a mirror dipole that changes its orientation at different sites above the protrusion.

the SNOM contrast can be understood intuitively by considering a tilted dipole being scanned across a protrusion, as shown schematically in Fig. 4(b). The tilted dipole induces a near-field mirror dipole of an orientation that changes with position. Above planar areas, the mirror dipole is perpendicular to the inducing dipole. On the edges of the protrusion, however, the mirror dipole is oriented antiparallel or collinear relative to the inducing dipole. This model offers a simple mechanism for the appearance of bright and dark spots at the boundaries of a homogeneous structure. The collinear mirror dipole is connected with a constructive interference and leads to an increase of the SNOM signal, whereas the antiparallel mirror dipole is connected with a destructive interference leading to a decrease. The following discussion shows that this effect may also lead to the complex asymmetric pattern and to the changes of bright and dark spots in the SNOM images of the gold projection sample.

In order to test our interpretation of the contrast of SNOM images recorded with a T-tip, numerical simulations of the scattering by an object of arbitrary shape locally excited by an oscillating electric dipole with a defined orientation were performed by means of the Green dyadic technique.[30] When the Green dyadic technique is used, the scatterer is discretized in direct space as an arrangement of small polarizable pieces of matter (cells) with dimensions much smaller than the wavelength of the incident light. With this assumption, the electric field inside each cell is supposed to be homogeneous and can thus be computed from the equation[31]

$$\mathbf{E}(\mathbf{r}_k) = \sum_l \mathbf{K}(\mathbf{r}_k, \mathbf{r}_l, \omega)\mathbf{E}_0(\mathbf{r}_l), \qquad (1)$$

where $\mathbf{r}_k$ denotes the center position of the kth cell and where $\mathbf{E}_0(\mathbf{r}_l)$ represents the incident field at the location of the lth cell. The tensor $\mathbf{K}$ is known as the generalized Green's tensor and can be deduced from the Green's dyadic $\mathbf{G}_0$ of the reference system by[32]

$$\mathbf{K} = (\mathbf{1} - \mathbf{G}_0\mathbf{V})^{-1}, \qquad (2)$$

with the potential $\mathbf{V}$ defined as

$$\mathbf{V} = \frac{\omega^2}{c^2}\Delta\epsilon\mathbf{1}, \qquad (3)$$

where $\mathbf{1}$ denotes the unit dyadic and $\Delta\epsilon$ denotes the dielectric-function contrast between the scatterer and the surrounding medium. The reference system described by $\mathbf{G}_0$ is the unperturbed system that would exist in the absence of the scatterers. In our case, because the samples

are embedded in a PC layer, we should consider the PC layer deposited onto the glass substrate as the reference system. However, to date, the components of the Green's dyadic of such a stratified medium are only known in an integral form,[33] leading to prohibitive computation times when dealing with scatterers described by more than a few cells. Because in our situation an accurate description of the shape of samples is necessary to model their near-field responses, we suppose for the calculations that the scatterers are embedded in a homogeneous medium instead of a stratified one. With this approximation, $\mathbf{G}_0$ is analytic, such that the generalized tensor $\mathbf{K}$ can be computed with a reasonable computation time, even for an object described by a large number of cells. Once $\mathbf{K}$ is known, it is a simple matter to model the dipole scanning over the scatterer. Indeed, if we suppose that the field $\mathbf{E}_0$ results from an oscillating dipole of constant moment $\mathbf{p}$ and located at $\mathbf{R}_p$, then the incident field at the position $\mathbf{r}_l$ in the absence of the scatterer is given by[34]

$$\mathbf{E}_0^{(R_p)}(\mathbf{r}_l) = \omega^2\mu_0\mathbf{G}_0(\mathbf{r}_l, \mathbf{R}_p)\mathbf{p}. \qquad (4)$$

With this definition, the electric field $\mathbf{E}^{(R_p)}$ due to the exciting dipole and existing inside each cell of the scatterer is directly calculated from Eq. (1). Applying an asymptotic form of $\mathbf{G}_0$[32] to this field $\mathbf{E}^{(R_p)}$ allows the calculation of the electric far field radiated coherently by both the exciting dipole and the sample. From this far field, one can compute the power radiated by the system into a given solid angle.[33] This radiated power is an attempt to model the optical signal collected by the microscope objective of our SNOM for a given position of the T-tip with respect to the sample. Obviously, we finally simulate the scanning of the T-tip by sweeping within a preset range the location of the exciting dipole.

The results displayed in Fig. 5 serve as a first example for the comparison of experiments with numerical simulations. We show in Figs. 5(c) and 5(e) an enlarged area of, respectively, the SFM image [Fig. 5(a)] and the simul-
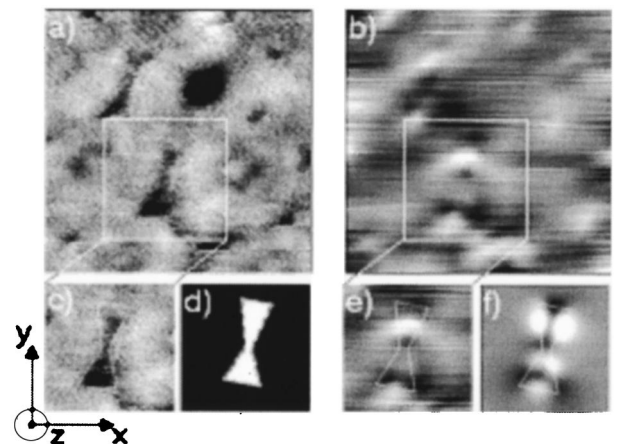

Fig. 5. Gold projection sample embedded in PC. The scan size is 480 nm × 480 nm. (a) SFM image; the gray scale corresponds to 4.3 nm. (b) Simultaneously recorded SNOM image (image contrast is 1%). (c), (e) Enlarged areas of (a) and (b), respectively. (d) Numerical object build up with (5 nm)^3 gold cells with a dielectric function $\epsilon = -8.80 + i1.09$. (f) Simulated SNOM image of the numerical object described in (d), the scanning dipole being tilted by 45° with respect to the sample surface and pointing into the negative y and positive z directions.

taneously recorded SNOM image [Fig. 5(b)] of a gold projection pattern.   Presumably due to an imperfection of the latex-bead mask,[27] the structure we consider is a gold patch where two triangles are connected [see Fig. 5(c)]. To model this structure, an object built up with 125-nm^3 cubic cells was numerically generated [Fig. 5(d)].   The white polygon displayed in Figs. 5(c), 5(e), and 5(f) represents the projection profile of this numerical structure. The thickness of this object was chosen to be 15 nm in order to fit with that of the experimental samples.   For all the calculations presented in this study, the sample was supposed to be embedded in a homogeneous medium with an optical index of 1.5 in order to account for the presence of the PC layer around the experimental samples.   An electric dipole, oscillating at a frequency corresponding to a wavelength of 635 nm in vacuum was scanned in a plane located 15 nm over the top of the object.   By recording for each position of the dipole the power radiated by the whole system into a solid angle of 0.38 sr, the image shown in Fig. 5(f) was obtained.

When comparing the two images of Figs. 5(e) and 5(f), one can observe a fairly good agreement between the experimental image and the computational one.   Indeed, two dark spots at the lower apexes and a bright region below the transition to the upper triangle can be distinguished in the SNOM image as well as in the calculated image, whereas the bright spot is a bit more pronounced in the calculation than in the experimental image.   For the upper region, the calculated and the experimental images show a dark spot right above the center of the structure and in the middle of the horizontal edge of the upper triangle.   In between these two dark regions, one can observe an intense bright area on the experimental image, whereas two bright spots are visible over the vertical edges of the upper triangle in the computed image.   Obviously, the deviation from the experimental values of many parameters, such as the dielectric function, the exact three-dimensional shape of the object, or even the scanning height, could explain this discrepancy.   In the SFM image the upper triangle seems to be smaller than the lower one and resembles a narrow bar.   It was verified that such a modification leads indeed to a merging of the two white spots.   It is, however, difficult to deduce the exact shape of the structure from the SFM image.   From this first comparison, we conclude that the contrast of the SNOM images taken with a T-tip can be at least qualitatively modeled by the interaction of the sample with the field of a tilted dipole.[35]   To demonstrate the versatility of the dipolar model, we analyze the results obtained with another object and displayed in Fig. 6.   Figures 6(a) and 6(b) correspond, respectively, to an enlargement of the SFM image and the SNOM images shown in Fig. 3.   The sample we consider is represented by two equilateral triangles facing each other.   The computed SNOM image [Fig. 6(d)] was obtained by use of the numerical object shown in Fig. 6(c).   As in the previous case, the exciting dipole was tilted 45° with respect to the scanning plane. The near-field response [Fig. 6(d)] of each triangle appears as two bright spots separated by a dark groove. The two bright spots can be observed for the right triangle of the experimental SNOM image [Fig. 6(b)].   The distance of the centers of the two spots is 55 nm, and their
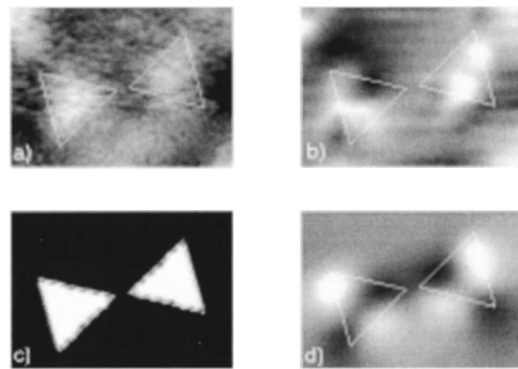

Fig. 6.   (a), (b) Enlarged areas of Fig. 3.   The scan size is 300 nm × 210 nm and corresponds to the upper-right rectangle displayed simultaneously in Figs. 3(a) and 3(b).   (c) Profile of the numerical sample.   (d) Simulated SNOM image of the object shown in (c).   The orientation of the dipole is similar to that used for Fig. 5(f).

full width at half-maximum (FWHM) with respect to the background intensity is 25 nm.   From this observation we conclude that the photonic nanopattern shows a two-point resolution of ∼50 nm and an edge resolution of the order of 25 nm.   The triangle on the left of Fig. 6(b) also shows a similarity to the calculated image.   Two well-separated dark spots in the experimental image correspond to a dark region with a constriction.   Conversely, two bright spots in the calculated image correspond to a bright region with a narrow constriction in the experimental result.   Overall, the dipolar character of the field emitted by the T-tip is evidenced by the qualitative agreement between the computed and the experimental contrast observed for both triangles.[36]   We remark that a SNOM experiment performed with a tip emitting a dipolar field can be interpreted as a direct "sensing" of the Green's dyadic of the sample.   Indeed, the Green's dyadic of an object is defined as the electromagnetic response of this object when excited by a dipolar field.   Thus, as shown by the results of this study, the complex relation between the structural properties of an object (e.g., shape and dielectric function) and the SNOM image taken with a dipolar tip is then directly encoded in the Green's tensor of the sample.   Therefore the use of a SNOM tip having a dipolar behavior could be of experimental interest for the direct measurement of the electromagnetic local density of states of nanoscopic samples.[37]

4.   CONCLUSION

The photonic nanopatterns of gold projection samples were investigated experimentally by scanning near-field optical measurements performed with a T-tip.   The experimental results have been compared with numerical calculations based on the Green's dyadic technique.   The strong dependence of the near-field images on the orientation of the T-tip with respect to the samples have been experimentally demonstrated.   A dipole tilted against the scanning plane has been used in the calculations to simulate the field emitted by a T-tip.   In view of this simple model and the complex structure of both the probe and the samples, a fairly good agreement between the experimental and the theoretical images has been found at a

resolution scale of better than 50 nm. From this qualitative agreement, we conclude that a T-tip behaves in the near-field mainly as a dipole having a significant moment component perpendicular to the surface of the sample. Such a specific feature of the T-tip could be of experimental interest in the context of selective local excitation of nanostructures such as metallic nanoparticles or even molecules.

ACKNOWLEDGMENT

REFERENCES

1. U. C. Fischer, "Scanning near-field optical microscopy," in *Scanning Probe Microscopy; Analytical Methods*, R. Wiesendanger, ed. (Springer-Verlag, Berlin, 1998).

2. E. H. Synge, "A suggested method for extending microscopic resolution into the ultramicroscopic region," Philos. Mag. **6**, 356–362 (1928).

3. E. A. Ash and G. Nicholls, "Super-resolution aperture scanning microscope," Nature **237**, 510–512 (1972).

4. D. W. Pohl, W. Denk, and M. Lanz, "Optical stethoscopy: image recording with resolution $\lambda/20$," Appl. Phys. Lett. **44**, 651–653 (1984).

5. U. C. Fischer, "Optical characteristics of 0.1 mm circular apertures in a metal film as light sources for scanning ultramicroscopy," J. Vac. Sci. Technol. B **3**, 386–390 (1985).

6. A. Dereux, G. Girard, and J. C. Weeber, "Theoretical principles of near-field optical microscopies and spectroscopies," J. Chem. Phys. **112**, 7775–7789 (2000).

7. T. Fujimura, T. Itoh, A. Imada, R. Shimada, T. Koda, N. Chiba, H. Muramatsu, H. Miyazaki, and K. Ohtaka, "Near-field optical images of ordered polystyrene particle layers and their photonic band effect," J. Lumin. **87–89**, 954–956 (2000).

8. S. A. Magnitskii, A. V. Tarasishin, and A. M. Zheltikov, "Near-field optics with photonic crystals," Appl. Phys. (N.Y.) **69**, 497–500 (1999).

9. Shanhui Fan, I. Appelbaum, and J. D. Joannopoulos, "Near-field scanning optical microscopy as a simultaneous probe of fields and band structure of photonic crystals: a computational study," Appl. Phys. Lett. **75**, 3461–3463 (1999).

10. O. J. F. Martin, "3D simulations of the experimental signal measured in near-field optical microscopy," J. Microsc. (Oxford) **194**, 235–239 (1999).

11. E. Betzig, J. K. Trautman, J. S. Weiner, T. D. Harris, and R. Wolfe, "Polarization contrast in near-field scanning optical microscopy," Appl. Opt. **31**, 4563–4568 (1992).

12. Th. Huser, L. Novotny, Th. Lacoste, R. Eckert, and H. Heinzelmann, "Observation and analysis of near-field optical diffraction," J. Opt. Soc. Am. A **16**, 141–148 (1999).

13. U. C. Fischer, J. Koglin, and H. Fuchs, "The tetrahedral tip as a probe for scanning near field optical microscopy at 30 nm resolution," J. Microsc. (Oxford) **176**, 231–237 (1994).

14. J. Koglin, U. C. Fischer, and H. Fuchs, "Material contrast in scanning near-field optical microscopy at 1–10 nm resolution," Phys. Rev. B **55**, 7977–7784 (1997).

15. J. Ferber, U. C. Fischer, N. Hagedorn, and H. Fuchs, "Internal reflection mode scanning near-field optical microscopy with the tetrahedral tip on metallic samples," Appl. Phys. A **69**, 581–589 (1999).

16. E. Betzig and J. Chichester, "Single molecules observed by near-field scanning optical microscopy," Science **262**, 1422–1428 (1993).

17. H. Gersen, M. F. Garcia-Parajo, L. Novotny, J. A. Veerman, L. Kuipers, and N. F. van Hulst, "Influencing the angular emission of a single molecule," Phys. Rev. Lett. **85**, 5312–5315 (2000).

18. U. C. Fischer, A. Dereux, and J. C. Weeber, "Controlling light confinement by excitation of localized surface plasmons," in *Near-Field Optics and Surface Plasmon Polariton*, S. Kawata, ed., Top. Appl. Phys. **81**, 49–69 (Springer-Verlag, Berlin, 2001).

19. J. Heimel, U. C. Fischer, and H. Fuchs, "SNOM/STM using a tetrahedral tip and a sensitive current-to-voltage converter," J. Microsc. (Oxford) **202**, 53–59 (2001).

20. P. Güthner, U. C. Fischer, and K. Dransfeld, "Scanning near-field acoustic microscopy," Appl. Phys. B **48**, 89–92 (1989).

21. K. Karraï and R. D. Grober, "Piezoelectric tip-sample distance control for near field optical microscopes," Appl. Phys. Lett. **66**, 1842–1844 (1995).

22. Th. Murdfield, U. C. Fischer, H. Fuchs, R. Volk, A. Michels, F. Meinen, and E. Beckman, "Acoustic and dynamic force microscopy with ultrasonic probes," J. Vac. Sci. Technol. B **14**, 877–881 (1996).

23. A. Naber, H.-J. Maas, K. Razavi, and U. C. Fischer, "A dynamic force distance control suited to various probes for scanning near-field optical microscopy," Rev. Sci. Instrum. **70**, 3955–3961 (1999).

24. A. Naber, "The tuning fork as sensor for dynamic force distance control in scanning near-field optical microscopy," J. Microsc. (Oxford) **194**, 307–310 (1999).

25. U. C. Fischer and H. P. Zingsheim, "Submicroscopic pattern replication with visible light," J. Vac. Sci. Technol. **19**, 881–885 (1981).

26. T. Kalkbrenner, M. Graf, C. Durkan, J. Mlynek, and V. Sandoghdar, "High-contrast topography-free sample for near-field optical microscopy," Appl. Phys. Lett. **76**, 1206–1208 (2000).

27. U. C. Fischer, J. Heimel, H.-J. Maas, M. Hartig, S. Höppener, and H. Fuchs, "Latex bead projection nanopatterns," Surf. Interface Anal. **33**, 75–80 (2002).

28. B. Hecht, H. Bielefeldt, Y. Inouye, D. W. Pohl, and L. Novotny, "Facts and artifacts in near-field optical microscopy," J. Appl. Phys. **81**, 2492–2498 (1997).

29. All SNOM images are flattened in the first order line by line to subtract slow changes of the laser intensity. The contrast of SNOM images is defined as the difference from the lowest to the highest signal normalized to the mean value in the image. This normalization represents an arbitrary choice of a reference signal. The gray scale is adjusted to cover the maximal contrast in the image.

30. C. Girard and A. Dereux, "Near-field optics theories," Rep. Prog. Phys. **59**, 657–699 (1996).

31. O. J. F. Martin, C. Girard, and A. Dereux, "Generalized field propagator for electromagnetic scattering and light confinement," Phys. Rev. Lett. **74**, 526–529 (1995).

32. O. J. F. Martin and N. B. Piller, "Electromagnetic scattering in polarizable backgrounds," Phys. Rev. E **58**, 3909–3915 (1998).

33. L. Novotny, B. Hecht, and D. W. Pohl, "Interference of locally excited surface plasmons," J. Appl. Phys. **81**, 1798–1806 (1997).

34. J. D. Jackson, *Klassische Elektrodynamik* (De Gruyter, Berlin, 1981).

35. We have also done numerical simulations for dipoles with a different angle with respect to the surface. The best correspondence between numerical and experimental images was achieved with a dipole tilted 45° to the scanning plane. A tolerance of ±10° can be stated, in which the photonic pattern does not change significantly.

36. One referee insisted that we cite in this context the research of Michaelis *et al.*[38] and of Sandoghdar.[39] They use a single molecule as a probe for light microscopy of a sample similar to ours but by a factor of 10 larger. Their image shows a pattern that varies with the orientation of the triangles.[38] They compared the image to simulated images extracted from unpublished data of O. Martin. The calculations performed with dipolar orientations within the scanning plane or perpendicular to the scanning plane reveal photonic nanopatterns that have a characteristic pattern. The experimental images[38] and the calculated images have the property in common that the pattern

differs for different orientations of the triangles. Sandogdhar concludes that a "quantitative comparison of calculations with the experimental results could reveal the dipole orientation."[39] No conclusion was drawn about the orientation of the dipole, and therefore it is not clear whether a photonic pattern in our sense was observed at all.

37. G. Colas des Francs, C. Girard, J. C. Weeber, C. Chicane, T. David, A. Dereux, and D. Peyrade, "Optical analogy to electronic quantum corrals," Phys. Rev. Lett. **86**, 4950–4953 (2001).
38. J. Michaelis, C. Hettich, J. Mlynek, and V. Sandogdhar, "Optical microscopy using a single-molecule light source," Nature **405**, 325–328 (2000).
39. V. Sandogdhar, "Trends and developments in scanning near-field optical microscopy," in *Nanometer Scale Science and Technology*, M. Allegrini, N. Garcia, and O. Marti, eds. (IOS Press, Washington D.C., 2001), pp. 60–115.